



# Solar North–South Asymmetry and Hilbert Transform Analysis

Heon-Young Chang 

Department of Astronomy and Atmospheric Sciences, Kyungpook National University, Daegu 41566, Korea

\*Corresponding Author: H.-Y. Chang, [hyc@knu.ac.kr](mailto:hyc@knu.ac.kr)

Received April 24, 2023; Accepted May 19, 2023; Published May 30, 2023

## Abstract

Here, we investigated the observed sunspot areas with respect to latitudes using the Hilbert transform technique. Conventional study of the cyclic patterns of sunspots is based on the Lomb–Scargle periodogram, which only obtains the amplitude information. In comparison, our approach characterizes the amplitude as well as the phase of solar activity. We demonstrated the solar North–South asymmetry in the instantaneous amplitude by analyzing daily sunspot data set spanning from the solar cycles 11 to 24. Our findings confirm that the northern hemisphere is dominant in the solar cycles 14, 15, 16, 18, and 20. Unlike the amplitude, the North–South asymmetry in the period of solar activity could not be established. We have also found that the standard deviation as a measure of fluctuation in the phase derivative is minimum in the latitude band  $10^\circ < l < 20^\circ$ , and the fluctuations obtained for latitudes above  $30^\circ$  are considerable.

**Keywords:** Sun: sunspot – Sun: activity – methods: data analysis

## 1. Introduction

Sunspots are used to trace magnetic flux tubes on the solar surface and thus provide the longest running records of solar magnetic activities. Based on the sunspots observed during the past centuries, the solar magnetic activity exhibits large variability in various timescales ranging from several days to hundreds of years (Schwabe 1843; Carrington 1860; Maunder 1890; Gleissberg 1971; Rieger et al. 1984; Pulkkinen et al. 1999; Bai & Sturrock 1991, 1993; Krivova & Solanki 2002; Usoskin 2017). The periodic characteristics of solar activity have been studied in details through the observations of magnetic field on the solar surface based on various magnetic proxies, such as, flare occurrence/index (Roy 1977; Ichimoto et al. 1985; Verma 1987; Joshi & Joshi 2004; Joshi & Pant 2005), coronal green-line (Tritakis et al. 1988), prominences/filaments (Hansen & Hansen 1975; Vizoso & Ballester 1989; Duchlev & Dermendjiev 1996; Duchlev 2001; Gigolashvili et al. 2005; Li 2010), sunspot groups (Li et al. 2002; Berdyugina & Usoskin 2003). The fact that each solar cycle with a period of  $\sim 11$  years is different from all others in shape has led the extensive study of solar cycle to predict its amplitude and duration. In these days, in particular, prediction of solar variation has emerged as an extremely hot topic in view of space weather forecasting (Petrovay 2010; Steenburgh et al. 2014; Jeong et al. 2020).

Further, observations reveal a statistically significant asymmetry in various indices of solar activity between the northern and southern hemispheres (Waldmeier 1971; Yi 1992;

Verma 1993; Carbonell et al. 1993; Ballester et al. 2005; Temmer et al. 2006; Zolotova & Ponyavin 2006; Chang 2008, 2012). The solar North–South asymmetry that varies on a time scale of solar cycles appears to be periodic and linked to the level of solar activity (White & Trotter 1977; Swinson et al. 1986; Knaack et al. 2004; Javaraiah 2007). Further study of this phenomenon has suggested that it is a fundamental characteristic of solar activity and is associated with the terrestrial space environment and the terrestrial climate changes (Egorova et al. 2000; Georgieva et al. 2007; Cho et al. 2011, 2012). This asymmetry can be explained through the interference between the dipolar and quadrupolar components of the solar magnetic field (Tobias 1997; Ossendrijver 2003; DeRosa et al. 2012; Shukuya & Kusano 2017).

In addition to sunspot records in time, the latitudinal variations of the sunspot-generating zone with time provide valuable information. Sunspots of a new solar cycle begin to form at approximately  $\pm 40^\circ$  in latitude (Hathaway 2011; Temmer et al. 2002, 2006; Zolotova & Ponyavin 2006, 2007; Ternullo 2007, 2010; Li et al. 2002, 2010; Solanki et al. 2008). This region drifts toward the equator as the solar cycle proceeds, resulting in the well-known butterfly diagram (Maunder 1904). While counting sunspots as a function of time, it should be borne in mind that the sunspots of a new solar cycle appear at mid-latitudes whereas the sunspots of the previous cycle are still developing near the equator. In other words, some sunspots in the ascending phase of a solar cycle are to be identified as belongings to the preceding solar cycle. Similarly,

sunspots at relatively higher latitudes in the descending phase should be regarded as belonging to the subsequent solar cycle. The study of the center-of-latitude of the observed sunspots with the area-weighted butterfly diagram revealed that the latitude distribution of sunspots follows a bimodal distribution and the solar activity level correlates with the median latitude of the spotting zone (Chang 2011). By exploring the relation between the latitudinal distribution of sunspots and solar activity, Chang (2022) has further demonstrated that the maximum International Sunspot Number strongly correlates with the average, standard deviation, skewness of the latitudinal distribution of sunspots.

The butterfly diagram based on magnetogram data shows additional intriguing features. For instance, there is clear evidence of poleward flux transport between the active and polar latitudes. Furthermore, there is the change of the polarity of the polar fields once each cycle near the maximum of solar activity, but not simultaneously at the north and south poles (Sun et al. 2015; Pishkalo 2019; Mursula et al. 2021). The regions exhibiting this phenomenon were first named as unipolar magnetic regions by Bumba & Howard (1969) and the phenomenon is now referred to as “rush to the poles”. If the active regions are tilted in the east-west direction, diffusion may lead to a net transport of flux of one polarity to the poles. The tilt angle between the spotting latitude and the line connecting the leading to following sunspots in bipolar sunspots is reported to increase with latitude, known as Joy’s law (Hale et al. 1919; Wang & Sheeley 1989; Howard 1991; Pevtsov et al. 2014).

Efforts of research on solar activity are focused on not only estimating the impact on the space environment of the Earth but also understanding the mechanisms for the physical processes that generate the solar magnetic field and induce its evolution. Since the invisible solar magnetic field causes and manifests itself as all the phenomena on the solar surface, including sunspots, it is essential to consider both statistical properties of spatial and temporal distributions of sunspots when developing diagnostic tools for any potential model. In solar dynamo, the motion of the electrically conductive solar plasma in the tachocline between the radiative core and the convective envelope generates the global magnetic field against ohmic dissipation, that governs the spatio-temporal evolution of solar activity (Parker 1955; Babcock 1961; Leighton 1969). Although a classical  $\alpha$ - $\Omega$  dynamo model considers differential rotation and convective flows as the basic ingredients, the theoretical understanding of the processes leading to the formation of sunspots is still limited. For instance, the efficiency of the poleward migration of the decayed magnetic flux by a surface meridional flow is lower than the observed drift of the sunspot zone (e.g., Mordvinov et al. 2022). Subsequently, the so-called Babcock-Leighton mechanism has been incorporated in the development of flux transport dynamo models (Wang et al. 1991; Dikpati & Charbonneau 1999; Nandy & Choudhuri 2001). Currently, there are several flux transport dynamo models based on separate effects, however, they require observational constraints for further elucidation.

In this paper we aim to characterize solar activity in terms

of amplitude and phase by employing the Hilbert transform technique, which can help determine instantaneous amplitude and instantaneous phase from an oscillatory time series. The observed sunspot data have been traditionally analyzed in the frequency domain through the periodogram analysis developed by Lomb and Scargle (Lomb 1976; Scargle 1982). Notwithstanding an appropriate tool for analyzing unevenly-spaced data, this approach intrinsically related to the fast Fourier transform and only obtains information on the amplitude and completely neglects the phase information by squaring its transformed complex function. Further, we compared the phase of variations in sunspot area data in the northern hemisphere with that in the southern hemisphere. To this end, we also attempted to compare the phase variations in different latitude bands. We calculated the instantaneous phase from the alternating sunspot area instead of the raw sunspot area to characterize the phases of solar activity in the two separate hemispheres and at different latitude bands. The cyclic behavior of solar activity is suggested to be synchronized such that the cycle phase, that is, the deviation of the epochs of activity minima or maxima from a strict periodicity, may appear to be a superposition of the perfect clock and a small random phase perturbation (e.g., Yule 1927; Dicke 1978). This is consequence of the memory of the dynamo process over several solar cycles. If a long-term phase stability compared to the duration of the activity cycle is recovered as a function of latitude, the implications of the solar dynamo model concerning the physical mechanism underlying the solar magnetic activity should result in the above mentioned attribute of the phase. This paper is organized as follows. We begin with a description of the data analyzed in the present paper and methods to obtain the Hilbert transform of the observed sunspot areas in Section 2. We present the instantaneous amplitude and the instantaneous frequency of two hemispheres in Section 3, and discuss latitudinal variations of the instantaneous frequency in Section 4. Finally, we summarize the results and provide a brief conclusion in Section 5.

## 2. Data and Hilbert Transform

From 1874 to 1976, the Royal Greenwich Observatory (RGO) has recorded daily sunspot areas measured in units of millionths of a hemisphere. Subsequently from 1977, the data have been compiled by the US Air Force (USAF) from its own Solar Optical Observing Network (SOON) with the help of the US National Oceanic and Atmospheric Administration (NOAA) from 1977. In an effort to carefully combine the RGO data with the more recent data by the Marshall Space Flight Center Solar Physics Division, the entire dataset has been made publicly ready. We have extracted sunspot area data for the present analysis from the NASA website<sup>1</sup>, where the daily sunspot data set including the position of appearance is available for individual years as ASCII text files. The analyzed data set covers from May 1874 to September 2016 spanning from the solar cycles 11 to 24, though the observed sunspot data for the solar cycles 11 and 24 was incomplete.

<sup>1</sup><http://solarscience.msfc.nasa.gov/greenwch.shtml>

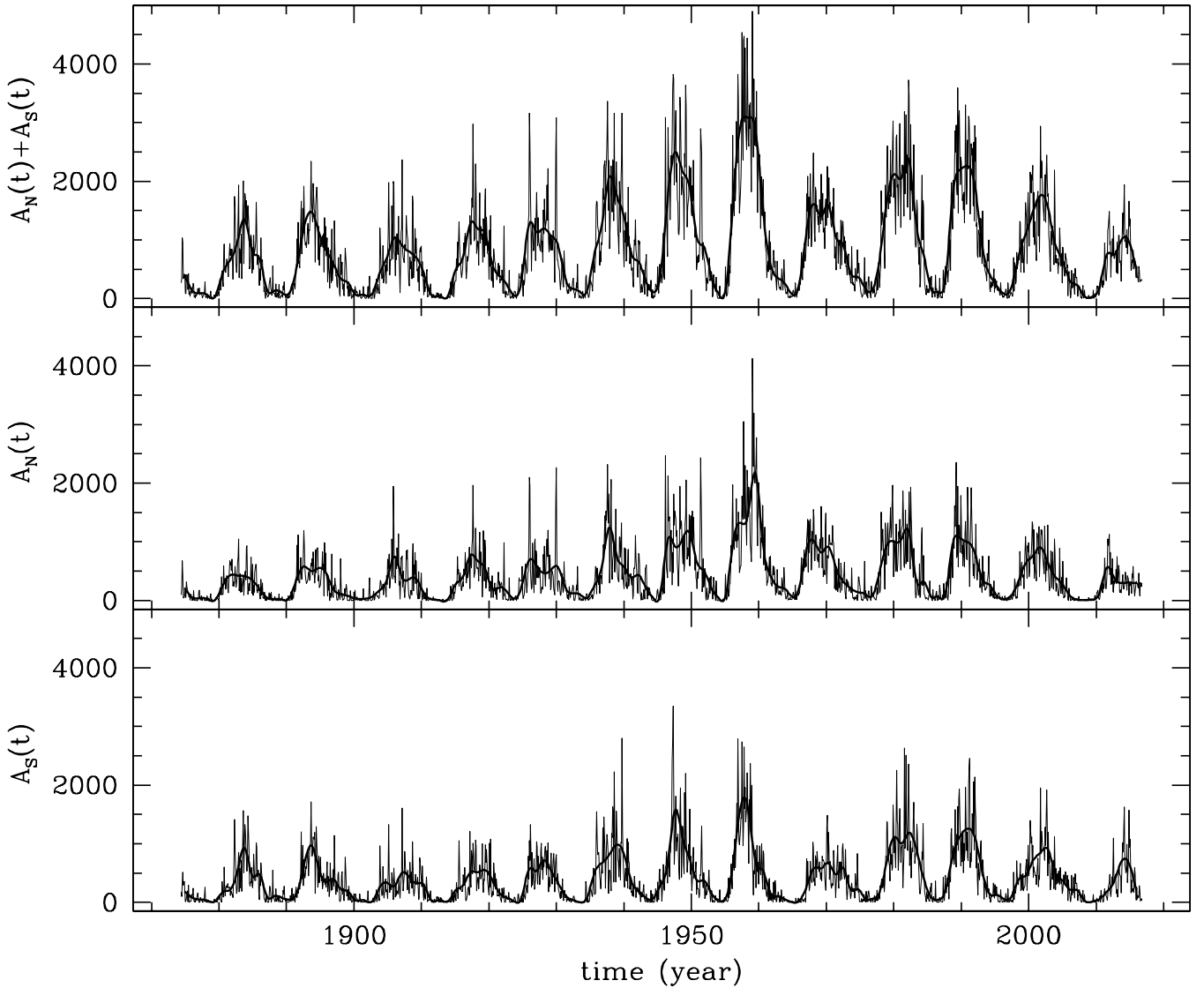


**Figure 1.** Observed sunspot areas. From top to bottom panel, thin curves represent the monthly averaged areas of the observed sunspots result from the sunspots appearing in the full disk, in the northern and southern hemispheres, respectively. The thick curves stand for the yearly sunspot area obtained using 13-month boxcar averages with 1-year steps.

In Figure 1, we show the monthly averaged areas of the observed sunspots appearing in the full disk, in the northern and southern hemispheres from top to bottom panel, respectively. The thick curves represent the yearly sunspot areas determined using 13-month boxcar averages with 1-year steps. As seen in Figure 1, the time series of the observed sunspot area repeatedly grows fast to its maximum and declines slowly to its minimum every  $\sim 11$  years. Instead of the raw sunspot area time series some researchers prefer conducting their study with a transformed index such as the Bracewell number (e.g., Dicke 1988; Kitiashvili 2016; Nagovitsyn & Pevtsov 2020). In the Bracewell representation the sunspot area is reversed with a sign change at the beginning of each solar cycle so that sunspot area is repeating with period of  $\sim 22$  years rather than  $\sim 11$  years (Bracewell 1953). In the original representation suggested by Bracewell, the odd solar cycles are assigned a negative sign. The underlying physical parameters, such as the toroidal magnetic field strength, appear to be related to

the Bracewell number in some nonlinear fashion. Moreover, underlying concept of this alternation can be accepted in terms of Hale’s polarity rule, which states that the magnetic field displays a periodicity of  $\sim 22$  years with a polarity inversion every  $\sim 11$  years (Hale 1908). The alternating sunspot area time series is also well motivated from the mathematical point of view in that the strongly peaked and asymmetrical sunspot data set strongly deviating from an unsophisticated sinusoidal curve is unfit for a mathematical technique extracting the phase of oscillating data. In Figure 2, as an example, we show the alternating sunspot area as a function of time obtained from the yearly sunspot area appearing in the full disk, which manifests a quasi-sinusoidal behavior.

Provided that the alternating sunspot area  $x(t)$  can be described as a solution of a damped harmonic oscillator’s equation such that

$$x(t) = \omega(t)^{-1/2} \sin \int \omega(t') dt', \quad (1)$$

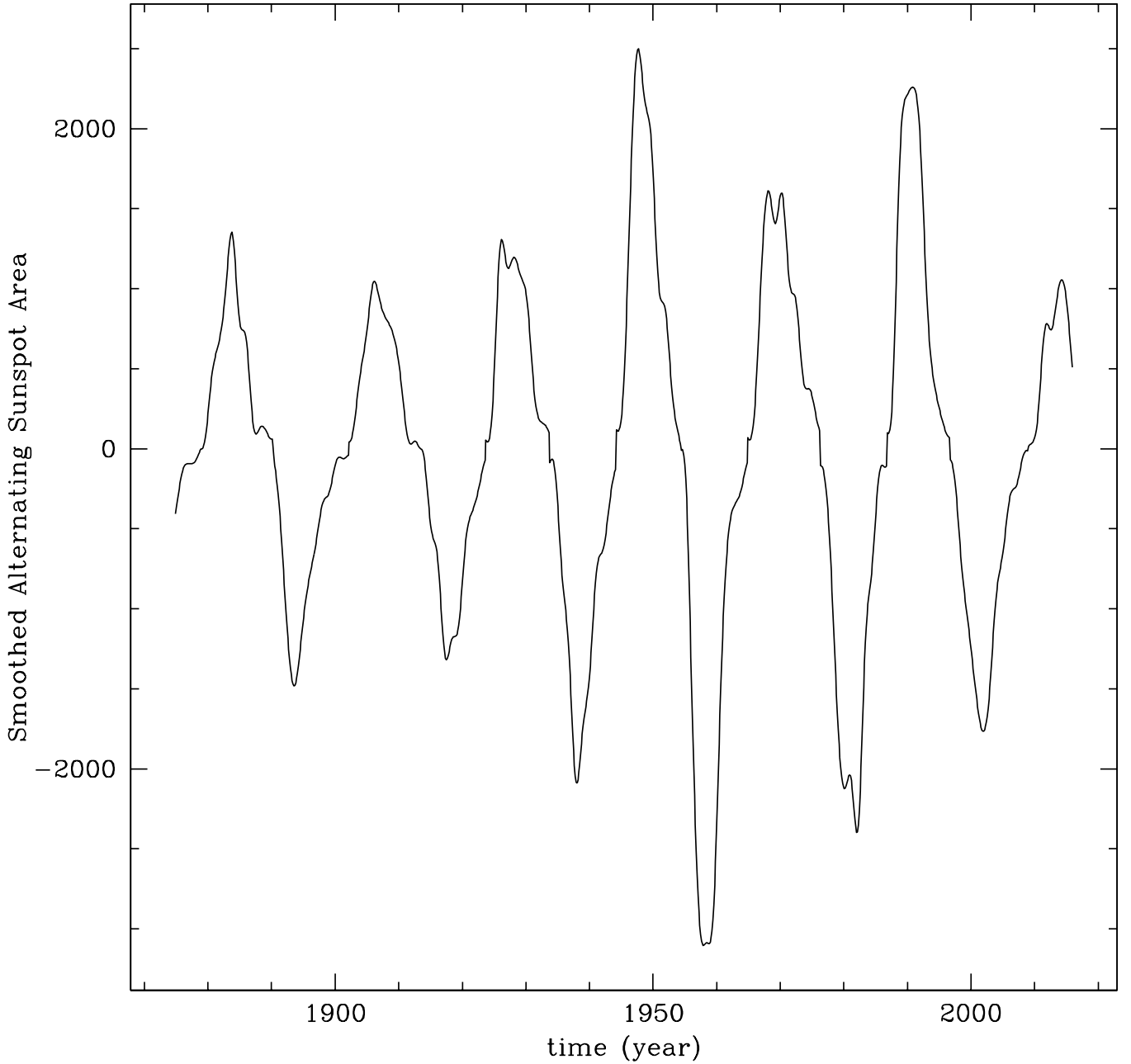


**Figure 2.** Alternating sunspot area as a function of time obtained from the yearly sunspot area appearing in the full disk

where  $\omega(t) = \omega_0 + \eta f(t)$ , the alternating sunspot area can be written as

$$x(t) = a(t) \sin \psi(t), \quad (2)$$

where  $\omega(t)$  is given as a time derivative of  $\psi(t)$ . Now, the cyclic frequency  $\nu_0$  is defined using  $\psi'(t) = \omega(t) = 2\pi\nu_0 + \delta(t)$  and calculated as a mean of  $\nu(t)$  over the time span.

For any function  $x(t)$ , its Hilbert transform  $\hat{x}(t)$  is defined as follows:

$$\hat{x}(t) = \frac{1}{\pi} P \int_{-\infty}^{\infty} \frac{x(\tau)}{t - \tau} d\tau, \quad (3)$$

where  $P$  denotes the Cauchy principal value of the singular integral. An analytic complex function  $z(t)$  is now given with the Hilbert transform  $\hat{x}(t)$  of the function  $x(t)$  as

$$z(t) = a(t)e^{i\phi(t)}, \quad (4)$$

where  $i = \sqrt{-1}$ . Here, the instantaneous amplitude  $a(t)$  and the instantaneous phase  $\phi(t)$  are given by

$$a(t) = \sqrt{x^2(t) + \hat{x}^2(t)}, \quad (5)$$

$$\phi(t) = \tan^{-1} \frac{\hat{x}(t)}{x(t)}, \quad (6)$$

respectively. Subsequently, the instantaneous frequency  $\omega(t)$  and the instantaneous period  $T(t)$  are obtained by

$$\omega(t) = \frac{d\phi(t)}{dt}, \quad (7)$$

$$T(t) = \frac{2\pi}{\omega(t)}, \quad (8)$$

respectively.

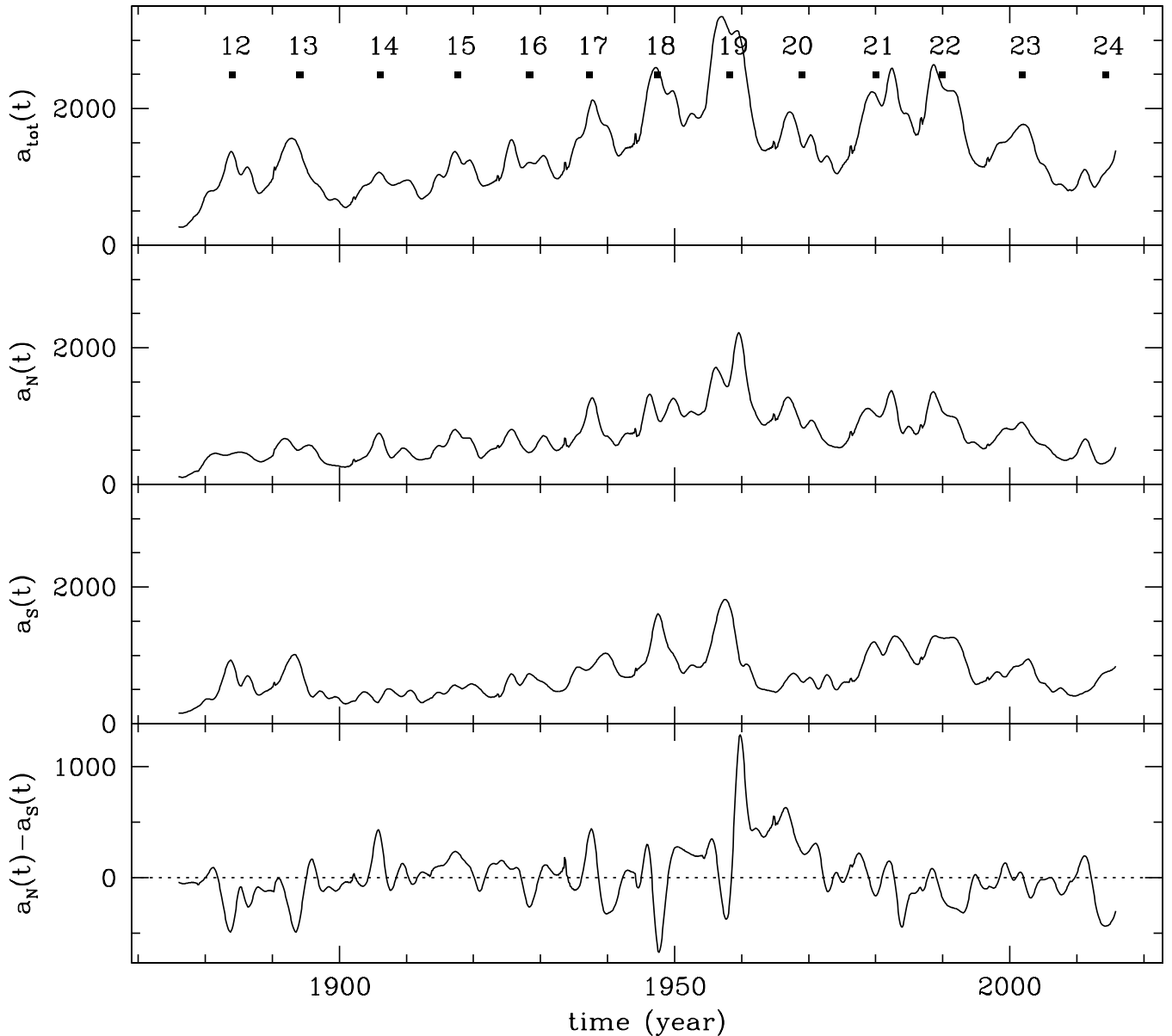


**Figure 3.** Instantaneous amplitude  $a(t)$ . The top panel shows the instantaneous amplitude of the sunspot area of the full disk. The second and third panels show the instantaneous amplitudes of the sunspot areas appearing separately in the northern and southern hemispheres, respectively. The bottom panel shows the difference between  $a_N(t)$  and  $a_S(t)$ . Note that the filled squares denote dates of the solar maximum with the corresponding solar cycle number.

### 3. Solar North-South Asymmetry in Instantaneous Amplitude and Instantaneous Frequency

In Figure 3, we show the instantaneous amplitude  $a(t)$  defined by Equation (5). In the top panel, the instantaneous amplitude resulting from the smoothed alternating sunspot area of the full disk is shown. In fact, this is equivalent to the envelope of the function plotted in Figure 2. It is noted that longer periodicities such as Gleissberg period ( $\sim 70$ – $100$  years) seems noticeable. In the second and third panels, the instantaneous amplitude calculated from the yearly averaged area of the sunspots separately appearing in the northern and southern hemispheres are shown, respectively. One may immediately notice two things: (1) two curves more or less resemble in appearance that shown

in the top panel, (2) the times at which the peaks appear do not exactly coincide. In the bottom panel, the difference between  $a_N(t)$  and  $a_S(t)$  is shown to better represent the North-South asymmetry of the observed sunspot area. The dotted horizontal line stands for the parity of the two hemispheres. Thus, when curves is located above the dotted line the northern hemisphere is more active, and vice versa. Our findings agree well with previous reports claiming that the solar northern hemisphere is dominant in the solar cycles 14, 15, 16, 18, 19 and 20 on average (e.g., Chang 2008; Javaraiah 2022). We should also like to point out that our attempt made here is novel in that a common procedure of comparing solar activity of two hemispheres is directly to subtract magnetic proxies obtained in two hemispheres.

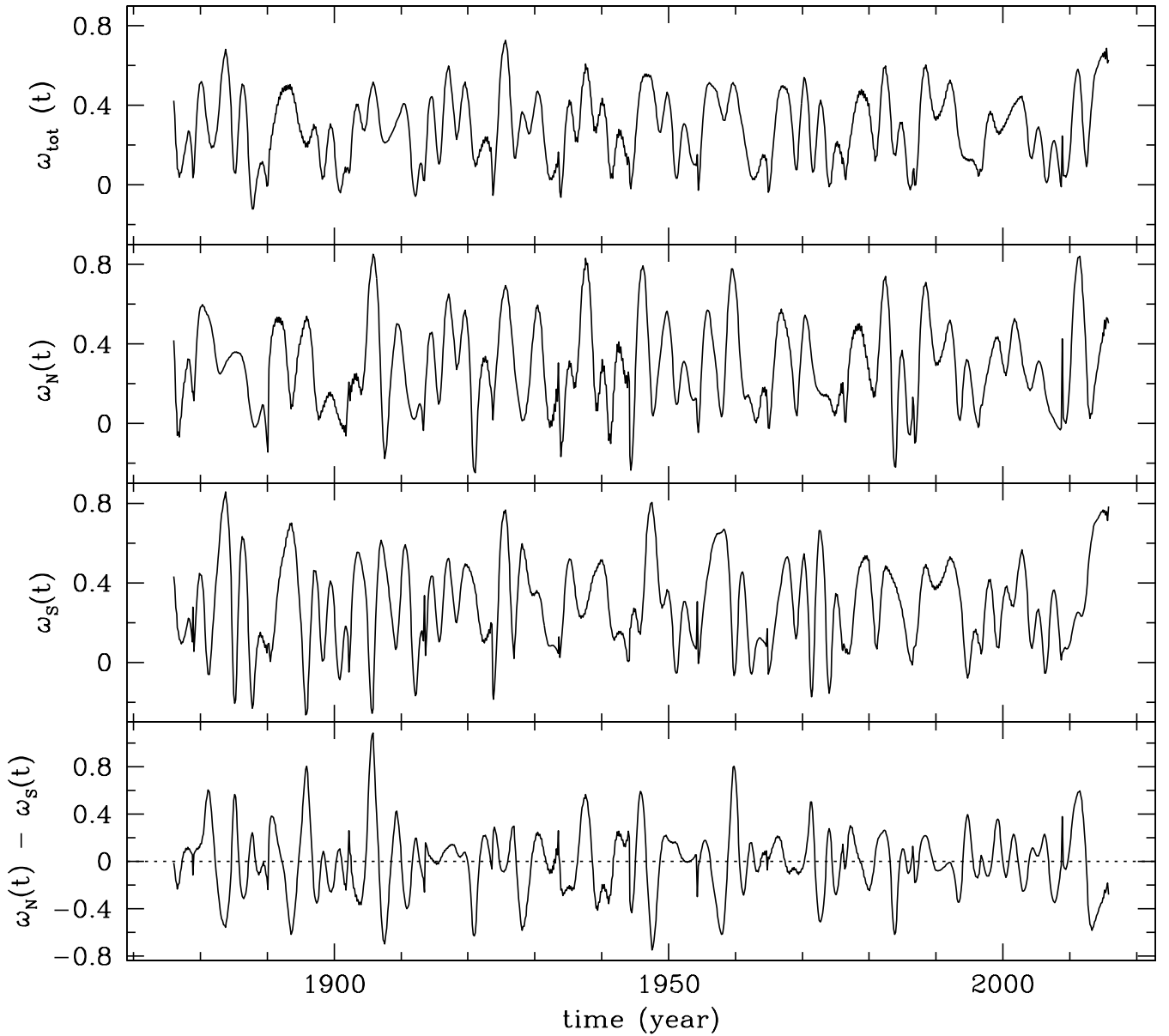


**Figure 4.** Derivative of the instantaneous phase  $\phi'(t)$ , or the instantaneous frequency  $\omega(t)$ . The second and third panels show the instantaneous frequencies of the sunspot areas appearing separately in the northern and southern hemispheres, respectively. The bottom panel shows the difference between  $\omega_N(t)$  and  $\omega_S(t)$ .

In Figure 4, we show the derivative of the instantaneous phase, or the instantaneous frequency  $\omega(t)$ , defined by Equations (6) and (7). From first to third panel,  $\omega(t)$  resulting from the smoothed areas of the sunspots appearing in the full disk, in the northern and southern hemispheres is shown, respectively. The difference between  $\omega_N(t)$  and  $\omega_S(t)$  is also shown in the last panel. The instantaneous frequency varies without abrupt wobbles throughout the solar cycles we have investigated, as if the solar cycle remembers a proper phase. The mean values of each  $\omega(t)$  in the case of the full disk, the northern hemisphere and southern hemisphere are 0.2857, 0.2843, and 0.2896  $\text{yr}^{-1}$ , respectively. They correspond to 21.99, 22.09, and 21.69 years in period, respectively. Unlike the case of the instantaneous amplitude, the periods of the two hemispheres are not quite different. As a measure of fluctuations, we have

further computed the standard deviations of  $\omega(t)$ , resulting in 0.1713, 0.2165, 0.2180 for the sunspots appearing in the full disk, in the northern and southern hemispheres, respectively. It is concluded that the North-South asymmetry is insignificant in the instantaneous frequency. In Table 1, we summarize the cyclic frequency  $\nu_0$ , the corresponding period  $P_0$  which is defined by the reciprocal of the cyclic frequency as  $1/\nu_0$ ,  $P_{0,1/2}$  which is a half of  $P_0$ , and the standard deviation of the instantaneous frequency  $\omega(t)$ .

#### 4. Latitudinal Variations of Instantaneous Frequency

In Figure 5, we show the monthly averaged sunspot area in thin curves, which appears only in the specific latitudinal band denoted in the upper right corner in each panel. The thick

**Table 1.** Cyclic frequency  $\nu_0$ , corresponding period  $P_0$ ,  $P_{0,1/2}$  which is a half of  $P_0$ , and the standard deviation of the instantaneous frequency  $\omega(t)$ .

	$\nu_0$ (yr <sup>-1</sup> )	$P_0$ (year)	$P_{0,1/2}$ (year)	Standard deviation
Full disk	0.0454	21.99	10.995	0.171
Northern hemisphere	0.0452	22.09	11.049	0.216
Southern hemisphere	0.0467	21.69	10.846	0.218

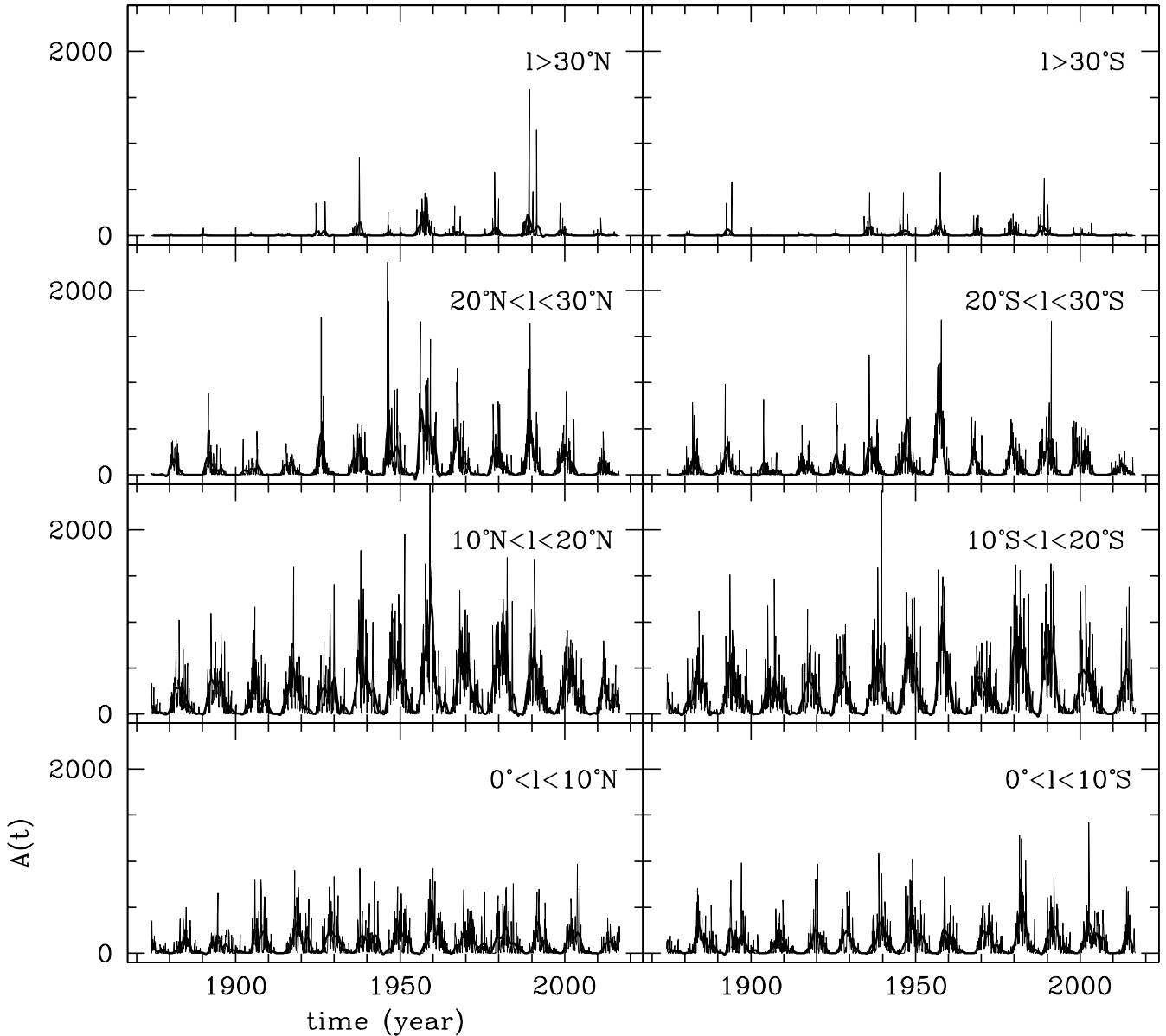


**Figure 5.** Sunspot area as a function of time. Note that it results from the sunspots only appearing in the specific latitudinal band denoted in the upper right corner in each panel.

curves represent the yearly sunspot areas determined using 13-month boxcar averages shown in Figure 1. The left and right columns of panels are results from the northern and southern hemispheres, respectively. As mentioned above, sunspots start to form at latitudes of  $\sim\pm 40^\circ$  when a new solar cycle begins and the sunspot-forming region is drifting equatorward as the solar cycle proceeds. Thus, in some sense the sunspots contributing to the plot in panels for the different latitude band

can be considered as those generated in a specific interval through ascending to descending phases of a given solar cycle in general. The comparison of corresponding panels in the two rows reveals the North-South asymmetry in terms of the observed sunspot area. In the top panels, the observed sunspot areas above  $\pm 30^\circ$  are trivial, unless solar cycles are particularly strong enough as in the Modern Maximum.

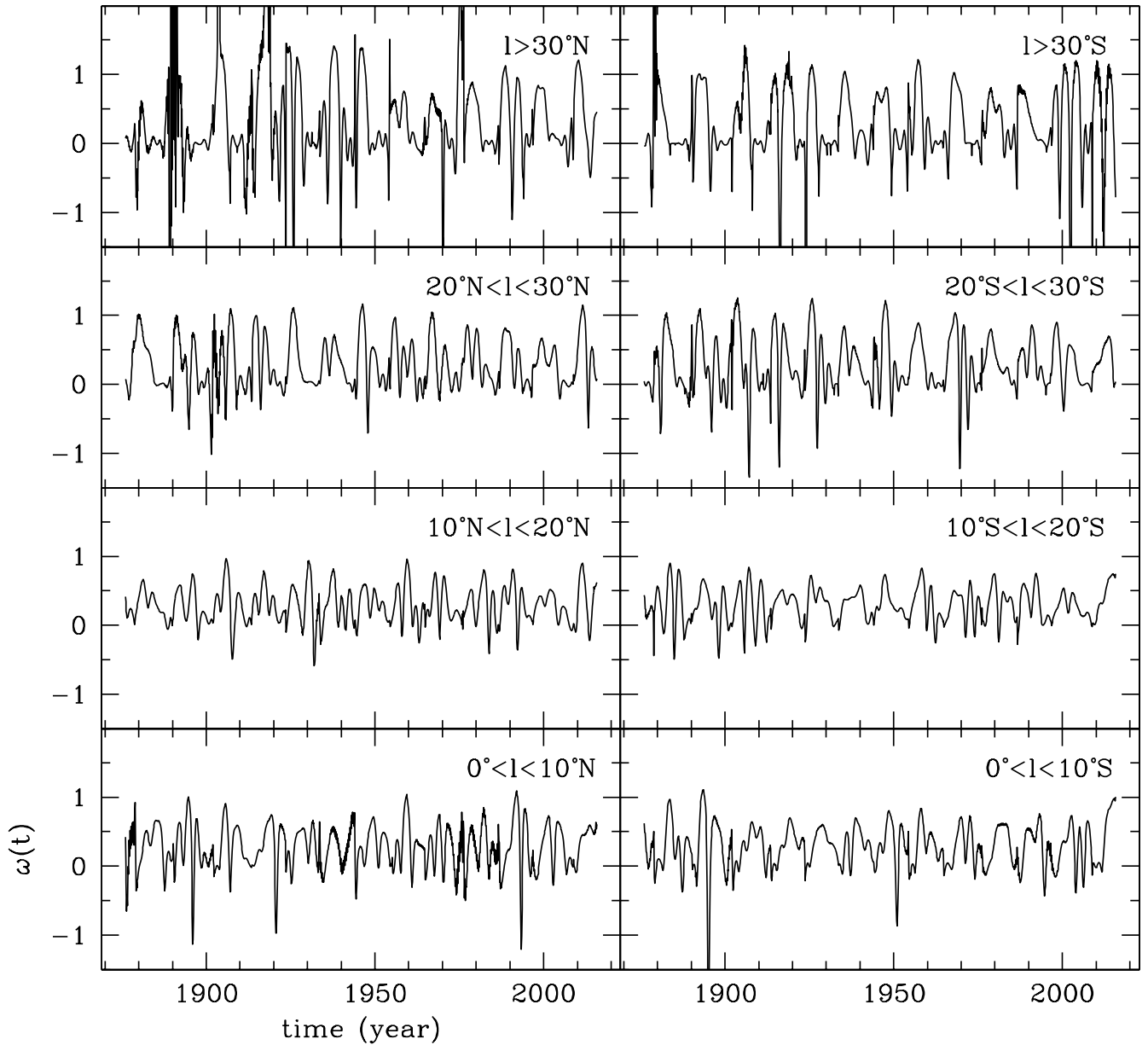


**Figure 6.** Instantaneous frequency  $\omega(t)$  for sunspot area appearing in different latitudinal bands denoted in the upper right corner in each panel.

In Figure 6, we show the instantaneous frequency  $\omega(t)$  for sunspot area appearing in the specific latitudinal band denoted in the upper right corner in each panel. Having alternated the yearly sunspot area using each panel in Figure 5, we calculated instantaneous amplitude and instantaneous frequency. In Table 2, we list the cyclic frequency  $\nu_0$ , and its reciprocal  $P_0$ , a half of  $P_0$ , and the standard deviation of the instantaneous frequency  $\omega(t)$ . As for the reciprocal of the cyclic frequency, any conspicuous trend as a function of the latitude band cannot be found. Besides, except the latitude band of  $l > 30^\circ$ , there is no sign of the North-South asymmetry of the instantaneous frequency in the corresponding latitude band. For comparison, in Figure 7, we show the Lomb-Scargle power spectrum computed from each panel in Figure 5. Based on the resulting Lomb-Scargle power spectra periodicities turn out to be rather regular, even for the latitude band of  $l > 30^\circ$ . We

note, however, that the recovered instantaneous frequency appears noisier than those shown in Figure 3, except the case of  $10^\circ\text{N} < l < 20^\circ\text{N}$  and  $10^\circ\text{S} < l < 20^\circ\text{S}$ . In particular, fluctuations in the instantaneous frequency obtained from latitudes above  $30^\circ$  in both hemispheres become quite large. Unlike the cyclic frequency, the standard deviation becomes the minimum in the band of  $10^\circ < l < 20^\circ$  and the maximum above  $l > 30^\circ$  for both hemispheres.

## 5. Summary and Conclusions

A cyclic pattern of sunspots with respect to time is produced by the variations in the magnetic fields generated in solar interior. A latitudinal distribution of sunspots including the North-South asymmetry is induced by the physical processes that stimulate variability in solar activity. Hence, the observed

**Table 2.** Cyclic frequency  $\nu_0$ , corresponding period  $P_0$ ,  $P_{0,1/2}$  which is a half of  $P_0$ , and the standard deviation of the instantaneous frequency  $\omega(t)$  for sunspot areas in different latitude bands.

	$\nu_0$ ( $\text{yr}^{-1}$ )	$P_0$ (year)	$P_{0,1/2}$ (year)	Standard deviation
$l > 30^\circ\text{N}$	0.0532	18.77	9.388	0.853
$20^\circ\text{N} < l < 30^\circ\text{N}$	0.0461	21.69	10.846	0.367
$10^\circ\text{N} < l < 20^\circ\text{N}$	0.0461	21.66	10.830	0.266
$0^\circ < l < 10^\circ\text{N}$	0.0441	22.65	11.329	0.329
$0^\circ < l < 10^\circ\text{S}$	0.0451	22.18	11.092	0.330
$10^\circ\text{S} < l < 20^\circ\text{S}$	0.0470	21.26	10.631	0.249
$20^\circ\text{S} < l < 30^\circ\text{S}$	0.0452	22.08	11.041	0.404
$l > 30^\circ\text{S}$	0.0447	22.34	11.174	0.581

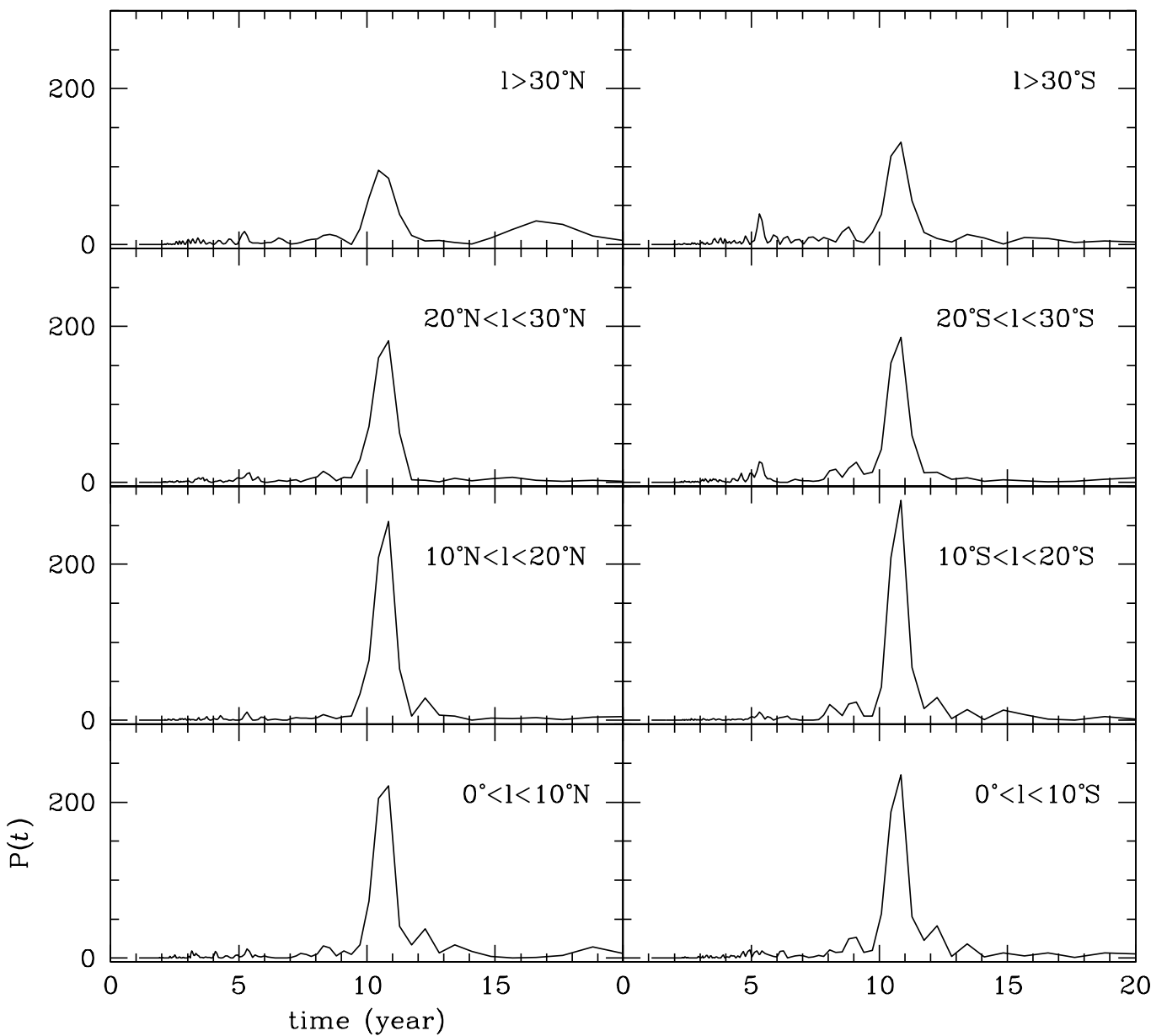


**Figure 7.** Lomb-Scargle power spectra computed from each panel provided in Figure 5.

solar variability in time and space should be carefully examined since proposed models of solar magnetic field generation are constrained by the observed distributions of sunspots. Here, we explored the temporal variability of the solar cycle in terms of sunspot area spanning from the solar cycles 11 to 24. With the Hilbert transform technique, we further characterized the phase of variations in data for sunspot areas in two hemispheres separately, and repeated the analysis with subgroups of different latitude bands.

We demonstrated the solar North-South asymmetry in the instantaneous amplitude, confirming that the northern hemisphere is dominant in the solar cycles 14, 15, 16, 18, and 20, as previously reported. It turns out that the instantaneous frequency varies without any abrupt changes throughout the solar cycles we investigated. Unlike the instantaneous amplitude, the North-South asymmetry in the instantaneous frequency could not be found. Additionally, no noticeable trend as a function of latitude bands was established in the cyclic frequency. Moreover, we found that the standard deviation was minimum in the latitude band  $10^\circ < l < 20^\circ$  and the fluctuations in the instantaneous frequency obtained from latitudes above  $30^\circ$  in both the hemispheres were considerable.

Therefore, it is suggested that the solar North-South asymmetry prevails in the instantaneous amplitude, but not in the instantaneous frequency. As far as the instantaneous frequency is concerned, both hemispheres seem to be modulated by a single phase-regulator. The variation in the instantaneous frequency may be dependent on latitude such that its fluctuation is minimum in the latitude band  $10^\circ < l < 20^\circ$ . Another finding to point out is that the instantaneous frequency varies without abrupt changes throughout the solar cycles from 11 to 24 even though the strength of the solar cycle changes with a period longer than several solar cycles. Further investigation is essential to determine whether this fact reflects the memory of the dynamo process over solar cycles.

## Acknowledgments

The author thanks the anonymous referees for critical comments and helpful suggestions which greatly improve the original version of the manuscript. This study was supported by a National Research Foundation of Korea Grant funded by the Korean government (NRF-2018R1D1A3B070421880) and Basic Science Research Program through the National Research Foundation (NRF) of Korea funded by the Ministry of Science, ICT and Future Planning (No. 2018R1A6A1A06024970).

## References

- Babcock, H. W. 1961, *ApJ*, 133, 572
- Bai, T., & Sturrock, P. A. 1991, *Nature*, 350, 141
- Bai, T., & Sturrock, P. A. 1993, *ApJ*, 409, 476
- Ballester, J. L., Oliver, R., & Carbonell, M. 2005, *A&A*, 431, L5
- Berdugina, S. V., & Usoskin, I. G. 2003, *A&A*, 405, 1121
- Bracewell, R. N. 1953, *Nature*, 171, 649
- Bumba, V., & Howard, R. 1969, *Sol. Phys.*, 7, 28
- Carbonell, M., Oliver, R., & Ballester, J. L. 1993, *A&A*, 274, 497
- Carrington, R. C. 1860, *MNRAS*, 20, 71
- Chang, H.-Y. 2008, *NewA*, 13, 195
- Chang, H.-Y. 2011, *NewA*, 16, 456
- Chang, H.-Y. 2012, *NewA*, 17, 247
- Chang, H.-Y. 2022, *JKAS*, 55, 139
- Cho, I.-H., Kwak, Y.-S., Chang, H.-Y., et al. 2011, *J. Atmos. Sol.-Terr. Phys.*, 73, 1723
- Cho, I.-H., Kwak, Y.-S., Marubashi, K., et al. 2012, *Adv. Space Res.*, 50, 777
- DeRosa, M. L., Brun, A. S., & Hoeksema, J. T. 2012, *ApJ*, 757, 96
- Dicke, R. H. 1978, *Nature*, 276, 676
- Dicke, R. H. 1988, *Sol. Phys.*, 115, 171
- Dikpati, M., & Charbonneau, P. 1999, *ApJ*, 518, 508
- Duchlev, P. I. 2001, *Sol. Phys.*, 199, 211
- Duchlev, P. I., & Dermendjiev, V. N. 1996, *Sol. Phys.*, 168, 205
- Egorova, L. V., Vovk, V. Y., & Troshichev, O. A. 2000, *J. Atmos. Sol.-Terr. Phys.*, 62, 955
- Georgieva, K., Kirov, B., Tonev, P., Guineva, V., & Atanasov, D. 2007, *Adv. Space Res.*, 40, 1152
- Gigolashvili, M. S., Japaridze, D. R., Mdzinarishvili, T. G., & Chargeishvili, B. B. 2005, *Sol. Phys.*, 227, 27
- Gleissberg, W. 1971, *Sol. Phys.*, 21, 240
- Hale, G. E. 1908, *ApJ*, 28, 315
- Hale, G. E., Ellerman, F., Nicholson, S. B., & Joy, A. H. 1919, *ApJ*, 49, 153
- Hansen, S. F., & Hansen, R. T. 1975, *Sol. Phys.*, 44, 503
- Hathaway, D. H. 2011, *Sol. Phys.*, 273, 221
- Howard, R. F. 1991, *Sol. Phys.*, 136, 251
- Ichimoto, K., Kubota, J., Suzuki, M., Tohmura, I., & Kurokawa, H. 1985, *Nature*, 316, 422
- Javaraiah, J. 2007, *MNRAS*, 377, L34
- Javaraiah, J. 2022, *Sol. Phys.*, 297, 33
- Jeong, H.-J., Moon, Y.-J., Park, E., & Lee, H. 2020, *ApJ*, 903, L25
- Joshi, B., & Joshi, A. 2004, *Sol. Phys.*, 219, 343
- Joshi, B., & Pant, P. 2005, *A&A*, 431, 359
- Kitiashvili, I. N. 2016, *ApJ*, 831, 15
- Knaack, R., Stenflo, J. O., & Berdyugina, S. V. 2004, *A&A*, 418, L17
- Krivova, N. A., & Solanki, S. K. 2002, *A&A*, 394, 701
- Leighton, R. B. 1969, *ApJ*, 156, 1
- Li, K. J. 2010, *MNRAS*, 405, 1040
- Li, K.-J., Liang, H.-F., & Feng, W. 2010, *Res. Astron. Astrophys.*, 10, 1177
- Li, K. J., Liang, H. F., Yun, H. S., & Gu, X. M. 2002, *Sol. Phys.*, 205, 361
- Lomb, N. R. 1976, *Ap&SS*, 39, 447
- Maunder, E. W. 1890, *MNRAS*, 50, 361
- Maunder, E. W. 1904, *MNRAS*, 64, 747
- Mordvinov, A. V., Karak, B. B., Banerjee, D., et al. 2022, *MNRAS*, 510, 1331
- Mursula, K., Getachew, T., & Virtanen, I. I. 2021, *A&A*, 645, A47
- Nagovitsyn, Y. A., & Pevtsov, A. A. 2020, *ApJ*, 888, L26
- Nandy, D., & Choudhuri, A. R. 2001, *ApJ*, 551, 576
- Ossendrijver, M. 2003, *A&A Rev.*, 11, 287
- Parker, E. N. 1955, *ApJ*, 122, 293
- Petrovay, K. 2010, *Living Rev. Sol. Phys.*, 7, 6
- Pevtsov, A. A., Berger, M. A., Nindos, A., Norton, A. A., & van Driel-Gesztelyi, L. 2014, *Space Sci. Rev.*, 186, 285
- Pishkalo, M. I. 2019, *Sol. Phys.*, 294, 137
- Pulkkinen, P. J., Brooke, J., Pelt, J., & Tuominen, I. 1999, *A&A*, 341, L43

- Rieger, E., Share, G. H., Forrest, D. J., et al. 1984, *Nature*, 312, 623
- Roy, J. R. 1977, *Sol. Phys.*, 52, 53
- Scargle, J. D. 1982, *ApJ*, 263, 835
- Schwabe, M. 1843, *Astron. Nachrichten*, 20, 283
- Shukuya, D., & Kusano, K. 2017, *ApJ*, 835, 84
- Solanki, S. K., Wenzler, T., & Schmitt, D. 2008, *A&A*, 483, 623
- Steenburgh, R. A., Biesecker, D. A., & Millward, G. H. 2014, *Sol. Phys.*, 289, 675
- Sun, X., Hoeksema, J. T., Liu, Y., & Zhao, J. 2015, *ApJ*, 798, 114
- Swinson, D. B., Koyama, H., & Saito, T. 1986, *Sol. Phys.*, 106, 35
- Temmer, M., Rybák, J., Bendík, P., et al. 2006, *A&A*, 447, 735
- Temmer, M., Veronig, A., & Hanslmeier, A. 2002, *A&A*, 390, 707
- Ternullo, M. 2007, *Sol. Phys.*, 240, 153
- Ternullo, M. 2010, *Ap&SS*, 328, 301
- Tobias, S. M. 1997, *A&A*, 322, 1007
- Tritakis, V. P., Mavromichalaki, H., & Petropoulos, B. 1988, *Sol. Phys.*, 115, 367
- Usoskin, I. G. 2017, *Living Rev. Sol. Phys.*, 14, 3
- Verma, V. K. 1987, *Sol. Phys.*, 114, 185
- Verma, V. K. 1993, *ApJ*, 403, 797
- Vizoso, G., & Ballester, J. L. 1989, *Sol. Phys.*, 119, 411
- Waldmeier, M. 1971, *Sol. Phys.*, 20, 332
- Wang, Y. M., & Sheeley, N. R., J. 1989, *Sol. Phys.*, 124, 81
- Wang, Y. M., Sheeley, N. R., J., & Nash, A. G. 1991, *ApJ*, 383, 431
- White, O. R., & Trotter, D. E. 1977, *ApJS*, 33, 391
- Yi, W. 1992, *JRASC*, 86, 89
- Yule, G. U. 1927, *Philos. Trans. Royal Soc. London Ser. A*, 226, 267
- Zolotova, N. V., & Ponyavin, D. I. 2006, *A&A*, 449, L1
- Zolotova, N. V., & Ponyavin, D. I. 2007, *A&A*, 470, L17